In Situ Electropolymerized Polypyrrole-based Molecularly Imprinted Polymer on a Screen-Printed Carbon Electrode for Preliminary Oxybenzone Detection

Nurshazwani Azim[1], Faizatul Shimal Mehamod[1,2]*, Nur Asyiqin Zulkefli[1], Mohd Azerulazree Jamilan[3], Azrilawani Ahmad @ Othman[1], Tengku Hasnan Tengku Abdul Aziz[4] and Eka Safitri[5]

[1]Faculty of Science and Marine Environment, Universiti Malaysia Terengganu, 21030 Kuala Nerus, Terengganu, Malaysia

[2]Advanced Nano Materials (ANoMA) Research Group, Faculty of Science and Marine Environment, Universiti Malaysia Terengganu, 21030 Kuala Nerus, Terengganu, Malaysia

[3]Nutrition Unit, Nutrition, Metabolism and Cardiovascular Research Centre, Institute for Medical Research, National Institute of Health, Ministry of Health Malaysia, No. 1, Jalan Setia Murni U13/52, Setia Alam, 40170 Shah Alam, Selangor, Malaysia

[4]Institute of Microengineering and Nanoelectronics, Universiti Kebangsaan Malaysia, 43600 Bangi, Selangor, Malaysia

[5]Department of Chemistry, Faculty of Mathematics and Natural Sciences, Universitas Syiah Kuala, Banda Aceh 23111, Indonesia

*Corresponding author (e-mail: fshimal@umt.edu.my)

Oxybenzone (benzophenone-3) is a widely used ultraviolet (UV) filter in sunscreen formulations; however, its release into aquatic environments poses serious risks to marine organisms. Conventional analytical techniques for oxybenzone detection are often costly, time-consuming, and require sophisticated instrumentation, highlighting the need for simple and portable sensing approaches. In this study, an *in situ* electropolymerized polypyrrole-based molecularly imprinted polymer (e-MIP) was developed on a screen-printed carbon electrode (SPCE) for oxybenzone detection, with a non-imprinted polymer (e-NIP) serving as a control. The electropolymerization process was carried out by cyclic voltammetry (CV) in the presence of oxybenzone as the template molecule, followed by template removal via a leaching process to generate selective recognition cavities. The fabricated e-MIP was characterized using scanning electron microscopy (SEM) and Fourier transform infrared (FTIR) spectroscopy, confirming the formation of the polypyrrole matrix and successful imprinting. Optimization studies indicated that optimal e-MIP performance was achieved using three electropolymerization scan cycles and a 10-minute incubation period at pH 7. Under optimal conditions, the e-MIP sensor demonstrated a reliable linear response to oxybenzone concentrations ranging from 5.0 to 25.0 mM. The limit of detection (LOD) and limit of quantification (LOQ) were calculated as 4.80 mM and 14.5 mM, respectively, utilizing the standard error of the regression. The proposed e-MIP demonstrated strong potential as a disposable, portable, and cost-effective sensor for oxybenzone detection.

Keywords: Oxybenzone. molecularly imprinted polymer, electropolymerization, screen-printed carbon electrode, cyclic voltammetry

Received: April 2026; Accepted: May 2026

Benzophenone-3, also known as oxybenzone, is an organic compound widely used in sunscreens and cosmetics to absorb harmful ultraviolet (UV) radiation. Despite its protective benefits for the skin, the extensive global use of oxybenzone has raised severe environmental and public health concerns. The compound continuously enters aquatic ecosystems during water-related recreational activities, where it acts as a potent pollutant and accumulates in environmental matrices [1, 2]. Oxybenzone has been identified as a major contributor to coral bleaching and bioaccumulation within marine food webs [3]. Furthermore, it is classified as a potential endocrine disruptor, posing systemic health risks and prompting outright bans in several environmentally sensitive marine regions [4].

Due to these threats, the strict monitoring of oxybenzone levels in aquatic environments is crucial. Conventional analytical techniques, such as ultrahigh-pressure liquid chromatography coupled with mass spectrometry (UHPLC-MS/MS), offer excellent sensitivity [5]. However, they are frequently hindered by high operational costs, lengthy sample preparation times, and a reliance on sophisticated, stationary laboratory equipment [6]. Therefore,

there is a strong need for faster, cost-effective, and precise alternative detection methods for immediate, on-site environmental monitoring [7].

Molecularly imprinted polymers (MIPs) combined with electrochemical detection offer a highly attractive and practical solution. Compared to bare electrochemical sensors, which often encounter electrode fouling in complex environmental matrices, MIPs provide enhanced selectivity and stability [8, 9]. The imprinting process involves co-polymerizing functional monomers around a specific target template molecule. Subsequent extraction of the template leaves behind highly tailored microcavities that match the target analyte's size, shape, and functional groups [10]. This "lock-and-key" mechanism gives MIPs exceptional binding specificity, making them superior to biological receptors in terms of physical, thermal, and chemical stability, as well as overall cost-effectiveness [11, 12].

While traditional MIPs are synthesized via bulk polymerization, *in situ* electropolymerization is uniquely advantageous for direct electrochemical sensor development [13, 14]. This technique enables the one-step deposition of a uniform polymer film directly onto an electrode surface under mild, aqueous conditions, circumventing the need for complex attachment chemistries [15]. By utilizing cyclic voltammetry (CV), researchers can rapidly regulate the film's thickness and morphology at the nanometre scale [16]. Conductive polymers like polypyrrole (PPy) are frequently selected as functional monomers because their electrochemical redox activity and electrical conductivity facilitate exceptional target recognition [17, 18].

Recent studies have successfully utilized *in situ* molecularly imprinted polypyrrole on screen-printed gold electrodes (SPGEs) for oxybenzone detection [19]. Building on these advancements, this work replaces expensive gold substrates with SPCEs to significantly improve cost-effectiveness and accessibility for routine analysis [20]. SPCEs are highly advantageous for *in situ* analysis because they facilitate system miniaturization, require only micro-sample volumes, and are highly suitable for mass production [21].

Herein, we report the development of an oxybenzone-specific electrochemical MIP (e-MIP) sensor using SPCEs for environmental monitoring. The molecular recognition interface was constructed via the CV-driven electropolymerization of pyrrole directly onto the SPCE surface. Following an optimized template extraction process, the structural and electrochemical properties of the resulting e-MIP cavities were extensively characterized. Finally, the sensor's analytical performance, including binding kinetics, linear dynamic range, and limits of detection, was systematically evaluated to assess its practical viability.

EXPERIMENTAL

Materials

Analytical-grade oxybenzone (≥98 %) and pyrrole (≥99 %) were purchased from Sigma-Aldrich. Hydrochloric acid (HCl), potassium ferrocyanide ($K_4[Fe(CN)_6]$), absolute ethanol, potassium chloride (KCl), and lithium perchlorate ($LiClO_4$) were obtained from R&M Chemicals. SPCEs were utilized as the primary electrochemical transduction platform. Deionized (DI) water, sourced from the institutional laboratory, was used throughout the study. Stocks of 10 mM oxybenzone and 100 mM pyrrole were prepared by dissolving the respective compounds in an 80:20 (v/v) mixture of absolute ethanol and DI water. The supporting electrolyte was prepared using 2 M lithium perchlorate in DI water.

Instrumentation

Electrochemical measurements, polymerization, and sensor calibrations were performed using a Methrohm Autolab PGSTAT302N potentiostat. Structural characterization of the polymers was conducted using an attenuated total reflectance-Fourier transform infrared (ATR-FTIR) spectrometer equipped with a platinum-diamond crystal. Surface morphology was analyzed using a Zeiss MERLIN Field Emission Scanning Electron Microscope (FESEM).

Procedures

Preparation of MIP and NIP Solutions

The MIP precursor solution was formulated by mixing equal volumes of the 10 mM oxybenzone stock, 100 mM pyrrole stock, 2 M electrolyte solution, and DI water to yield a total volume of 1 mL. The NIP control solution was prepared using an identical procedure, with the complete omission of the oxybenzone template.

Electrochemical Polymerization of Pyrrole Modified SPCE

Prior to modification, the bare SPCE was pre-treated in 1.0 M of H_2SO_4 for 2 minutes. To fabricate the sensor, 5 µL of the MIP solution was drop-casted onto the SPCE working area and incubated for 5 to 10 minutes to allow the spontaneous rearrangement of monomers around the template. Then, electrochemical polymerization was performed via CV by applying scans from -0.3 V to 0.9 V at a scan rate of 100 mV/s. The template was subsequently extracted by immersing

the modified electrode in a 0.1 M ethanolic HCl solution for 10 minutes. The electrode was then

vigorously washed with DI water to remove any residual acid and template. To ensure a valid comparison, the e-NIP control electrodes were fabricated using the NIP solution and were subjected to the exact same electropolymerization and 0.1 M ethanolic HCl leaching procedures.

Electrochemical Detection of Oxybenzone

To establish the baseline signal, 50 µL of 5 mM $[Fe(CN)_6]^{3-/4-}$ in 0.1 M KCl was drop-casted onto the modified SPCE. The electrochemical response was recorded using CV. The electrode was then washed with DI water and dried. Next, 5 µL of target samples or standards were incubated on the working electrode for 10 minutes. Following incubation, the electrode was washed and air-dried at room temperature. A fresh 50 µL aliquot of the redox probe was applied, and a subsequent CV scan was performed. The final analytical signal was determined by evaluating the change in the anodic peak current relative to the initial baseline measurement.

Morphological and Structural Characterization

ATR-FTIR spectra were recorded from 500 to 4000 cm^{-1} with 24 scans per sample. A blank sample holder was used to establish the background spectrum prior to capturing the absorption profiles. For surface morphology, the SPCE samples were thoroughly dried, mounted onto compatible substrates, and imaged at magnifications of 1500×, 3500×, 5000×, and 10,000× to assess particle size, surface roughness, and porosity.

Optimization of Sensor Fabrication and Operation

To maximize analytical performance, the template-to-monomer ratio was evaluated using varying oxybenzone concentrations (5, 10, 15, 20, and 25 mM) against a constant 100 mM pyrrole concentration. Target binding kinetics were then assessed across different post-electropolymerization incubation periods. Finally, the influence of pH on oxybenzone binding was investigated using supporting electrolytes adjusted from pH 3 to 11.

RESULTS AND DISCUSSION

Electropolymerization of the e-MIP

The molecularly imprinted polymer (MIP) was fabricated via the direct electropolymerization of pyrrole onto the SPCE surface. The precursor solution contained 100 mM pyrrole as the functional monomer and 10 mM oxybenzone as the template. CV was employed for film deposition, as the precise regulation of applied potential and scan cycles critically influences the sensor's final thickness, selectivity, and sensitivity.

Figure 1 illustrates the cyclic voltammograms recorded during the electropolymerization process. During the first forward scan, a distinct broad anodic oxidation peak was observed at approximately +0.45 V. This peak corresponds to the initial oxidation of pyrrole monomers into radical cations, which initiates the polymerization cascade [22]. As successive CV scans were performed (from the 1st to the 5th cycle), the anodic peak current decreased significantly and progressively. This characteristic attenuation confirmed the successful and continuous deposition of the molecularly imprinted polypyrrole film on the electrode surface.

As the polymer layer grows, it forms an increasingly resistive barrier that restricts electron transfer and redox access to the electrode surface. This progressive signal suppression across consecutive cyclic voltammograms is a well-documented phenomenon in MIP fabrication, demonstrating that the template molecules are successfully entrapped within the growing polymer matrix to generate specific recognition sites [17]. During this oxidative electropolymerization process, the synthesized polypyrrole backbone is inherently p-doped, yielding a positively charged polymer surface that is charge-balanced by the incorporation of perchlorate (ClO_4^-) counter-anions from the supporting electrolyte [23]. Furthermore, this dense polymer barrier provides tuneable surface properties that inherently resist non-specific biofouling in complex aqueous environments [24]. Ultimately, this single-step *in situ* electropolymerization process is analytically efficient and circumvents the use of hazardous organic solvents typically required in traditional bulk polymerization methods, validating the eco-friendly profile of the developed sensing platform [25].

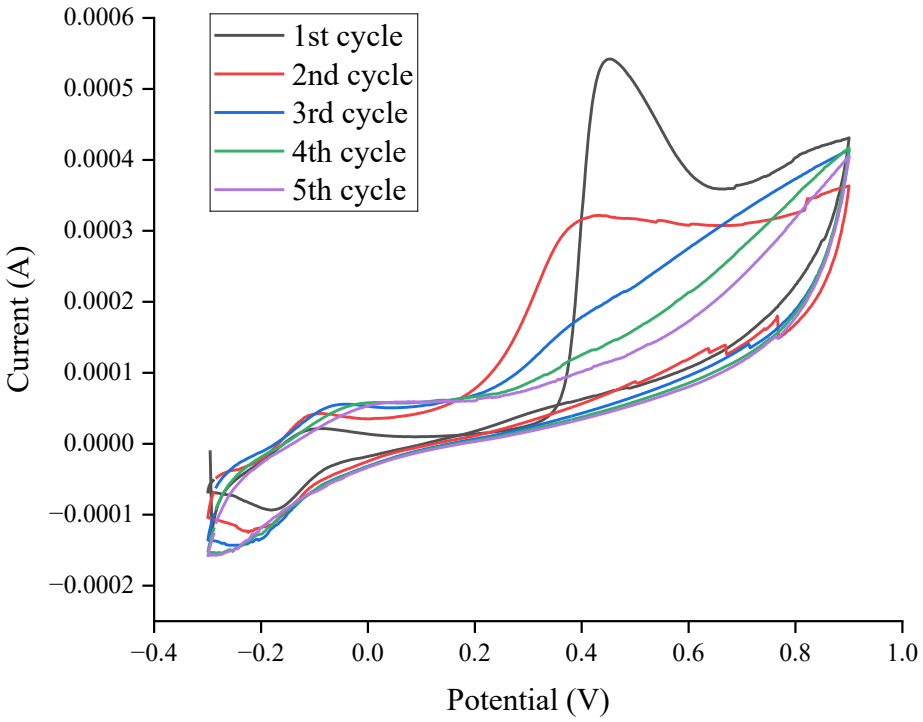

Figure 1. Cyclic voltammograms illustrating the electropolymerization of the SPCE polymer layer across the 1st, 2nd, 3rd, 4th and 5th scan cycles.

Electrochemical Behaviour of e-MIP and e-NIP

To verify the successful synthesis and functionality of the sensors, their electrochemical responses were evaluated by comparing the cyclic voltammograms at various fabrication stages, utilizing a 5.0 mM $[Fe(CN)_6]^{3-/4-}$ redox probe (Figure 2). Initially, the bare SPCE exhibited minimal faradaic activity, recording the lowest anodic peak current (I_{pa}). Following electropolymerization, both the e-NIP and the leached e-MIP exhibited significantly enhanced current responses compared to the bare electrode, confirming the successful deposition of the conductive polypyrrole films. Notably, the leached e-MIP demonstrated a lower anodic peak current than the e-NIP control. This decrease can be attributed to the extraction of the bulky oxybenzone template, which leaves behind a highly porous microcavity network. While these cavities are essential for target recognition, their empty, non-conductive voids temporarily disrupt the continuous electron transfer pathways of the polypyrrole matrix compared to the denser, highly conjugated layer of the e-NIP [26].

Upon incubation with the target analyte, the e-MIP's electrochemical profile exhibited a dramatic increase in anodic current. Because oxybenzone is inherently electroactive and oxidizes within a similar potential window, the sensor operates via a signal enhancement mechanism [27]. The tailored microcavities within the e-MIP specifically pre-concentrate the oxybenzone molecules directly at the electrode interface. During measurement, the direct electrochemical oxidation of this captured oxybenzone overlaps synergistically with the oxidation of the $[Fe(CN)^6]^{3-/4}$ redox probe. As clearly demonstrated by the cyclic voltammograms in Figure 2, the incubated e-MIP recorded the highest overall anodic peak current, definitively confirming the successful accumulation and direct oxidation of the target analyte within the customized polymer network [17]. Conversely, the incubated e-NIP displayed a significantly lower current response. Due to the complete absence of tailored recognition cavities, the continuous e-NIP polymer matrix cannot effectively capture or pre-concentrate the oxybenzone molecules, resulting in only minimal non-specific surface adsorption. This stark contrast in post-incubation electrochemical behaviour further validates the successful imprinting effect and superior affinity of the e-MIP.

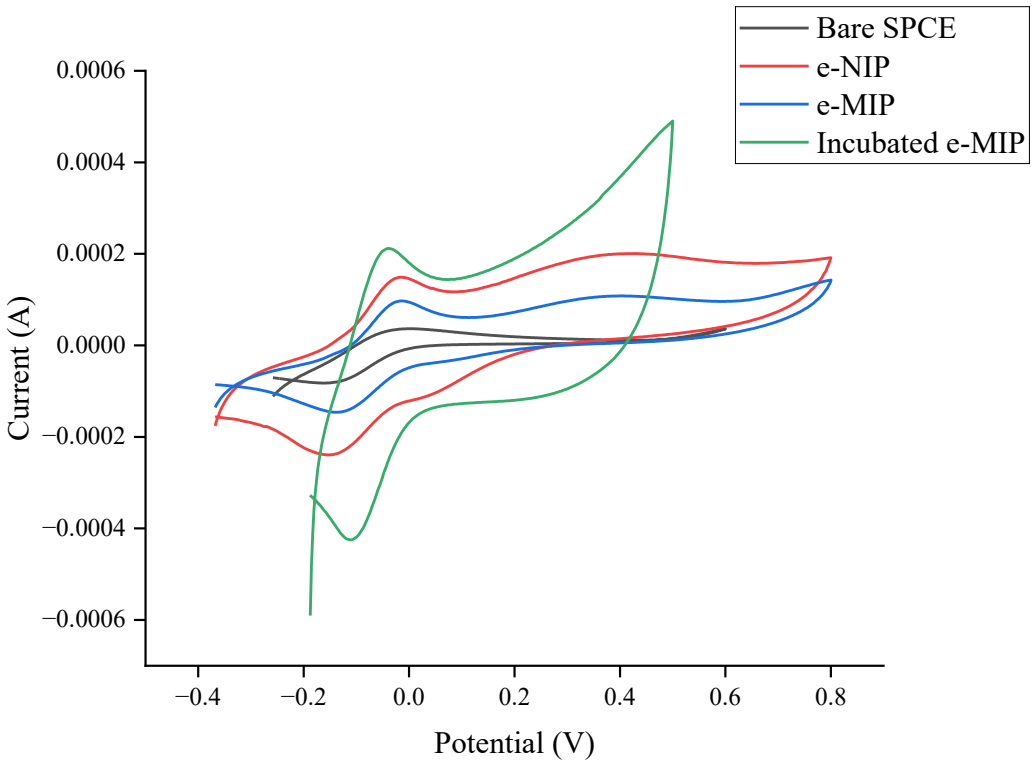

Figure 2. Cyclic voltammograms of the bare SPCE, e-NIP, leached e-MIP, and incubated e-MIP, recorded in 5.0 mM $[Fe(CN)_6]^{3-/4-}$ containing 0.1 M KCl.

Beyond structural complementarity, the exceptional selectivity is heavily influenced by the analyte's inherent hydrophobicity. Oxybenzone is a highly lipophilic compound (logKow = 3.79), which actively drives the target molecules out of the aqueous matrix and into the compatible polymer cavities, favouring polymer-analyte affinity over water-analyte interactions [28, 29]. Maintaining this stringent selectivity is paramount for real-world environmental applications. In aquatic ecosystems, biological remediation actively metabolizes oxybenzone into structurally analogous degradation products, such as 2,4-dihydroxybenzophenone. The customized microcavities of the e-MIP ensure the sensor distinguishes the intact UV filter from these environmental byproducts [8]. Furthermore, the rigid structure of the electropolymerized polypyrrole preserves the "permanent memory" of the imprinted cavities, ensuring they remain highly accessible for rapid and stable target accumulation [12, 13].

Characterization

Fourier Transform Infrared Spectroscopy (FTIR)

Fourier Transform Infrared (FTIR) spectroscopy was employed to monitor structural changes and functional group interactions during the imprinting, leaching, and rebinding stages. This technique provides molecular-level confirmation of polymerization and template removal by tracking the attenuation of characteristic functional peaks [30].

As illustrated in Figure 3, the unmodified bare electrode (black line), the leached e-NIP (blue line), and the leached e-MIP (green line) exhibited relatively featureless baseline absorption profiles, typical of the carbon substrate and thin polymer films. In contrast, the spectrum of the pure oxybenzone template (red line) displayed distinct characteristic markers. A broad absorption band between 3200 and 3400 cm^{-1} corresponds to phenolic -OH stretching, while peaks in the 2800–3000 cm^{-1} region are attributed to aliphatic and aromatic C-H stretching. Furthermore, the C=O stretching band was distinctly located at 1633 cm^{-1}, and aromatic C=C stretching bands were observed at 1593, 1506, and 1434 cm^{-1} [31].

Following template extraction, the leached e-MIP spectrum (green line) showed a near-complete absence of these specific oxybenzone markers, confirming the successful removal of the template to expose the recognition cavities. A minor residual signal in the C-H stretching region (2800–3000 cm^{-1}) suggests that a negligible fraction of the template remained permanently entrapped within the highly cross-linked polymer matrix, a common occurrence where solvent diffusion is restricted.

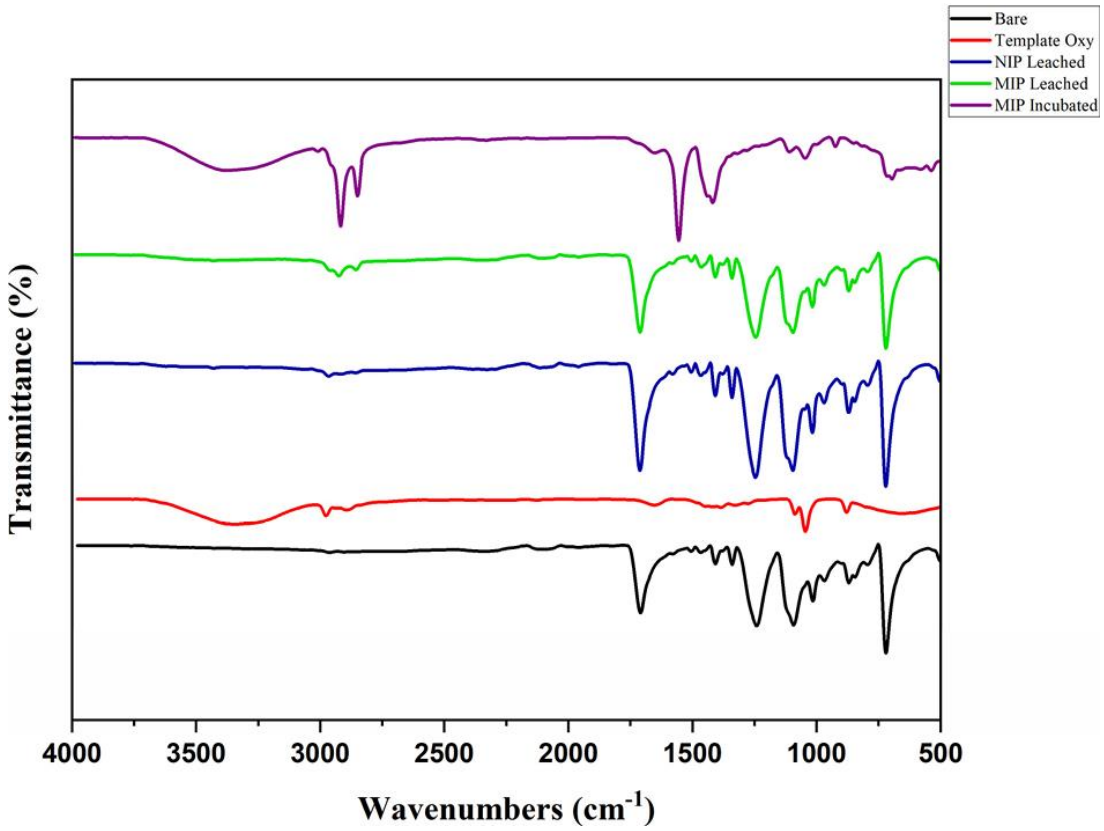

Figure 3. FTIR spectra of bare SPCE, oxybenzone, leached e-NIP, leached e-MIP, and incubated e-MIP.

Upon incubation with the target analyte, the e-MIP spectrum (purple line) revealed the prominent reappearance of oxybenzone's characteristic peaks, including the intense -OH stretch, the C-H stretching doublet, and the distinct C=O (1633 cm^{-1}) and C=C vibrations. The remarkable intensity of these peaks, which closely mirrors the pure template spectrum, substantiates the successful and dense accumulation of the analyte at the sensor interface. This high localized concentration is driven by specific non-covalent interactions within the tailored microcavities, including strong hydrogen bonding networks between the functional groups of the polymer and the analyte [28], further stabilized by dipole interactions and π-π stacking facilitated by the aromatic rings [8, 31].

Scanning Electron Microscopy (SEM)

The surface morphology of the modified electrodes was evaluated using scanning electron microscopy (SEM) to visually confirm the formation of the imprinted polymer and the structural changes following the leaching and rebinding processes.

As shown in Figure 5, the electropolymerization of pyrrole in the absence of the template yielded the leached e-NIP (Figure 4a), which displayed a densely packed, agglomerated globular structure typical of polypyrrole. This compact morphology is expected, as the absence of the template molecule during polymerization results in a continuous polymer lacking specific recognition cavities. Upon target exposure, the incubated e-NIP (Figure 4b) exhibited minimal morphological differences from its leached counterpart, corroborating the absence of specific binding interactions and highlighting its low affinity for the target.

In contrast, electropolymerization in the presence of oxybenzone profoundly altered the polymer architecture. Following template extraction, the leached e-MIP (Figure 4c) revealed a significantly rougher, highly porous nanostructure compared to the e-NIP. This morphological contrast is a hallmark of successful molecular imprinting, confirming the elimination of the template and the subsequent formation of specific recognition cavities [32]. This structural transformation is consistent with observations in other polypyrrole-based MIPs, where template removal yielded a distinctly porous surface containing numerous cavities compared to the compact structure of non-imprinted films [33, 34]. The creation of these specific recognition sites, tailored precisely to the size, shape, and functional groups of oxybenzone, significantly increases the electroactive surface area, thereby enhancing the polymer's binding capacity and facilitating efficient mass transport [35].

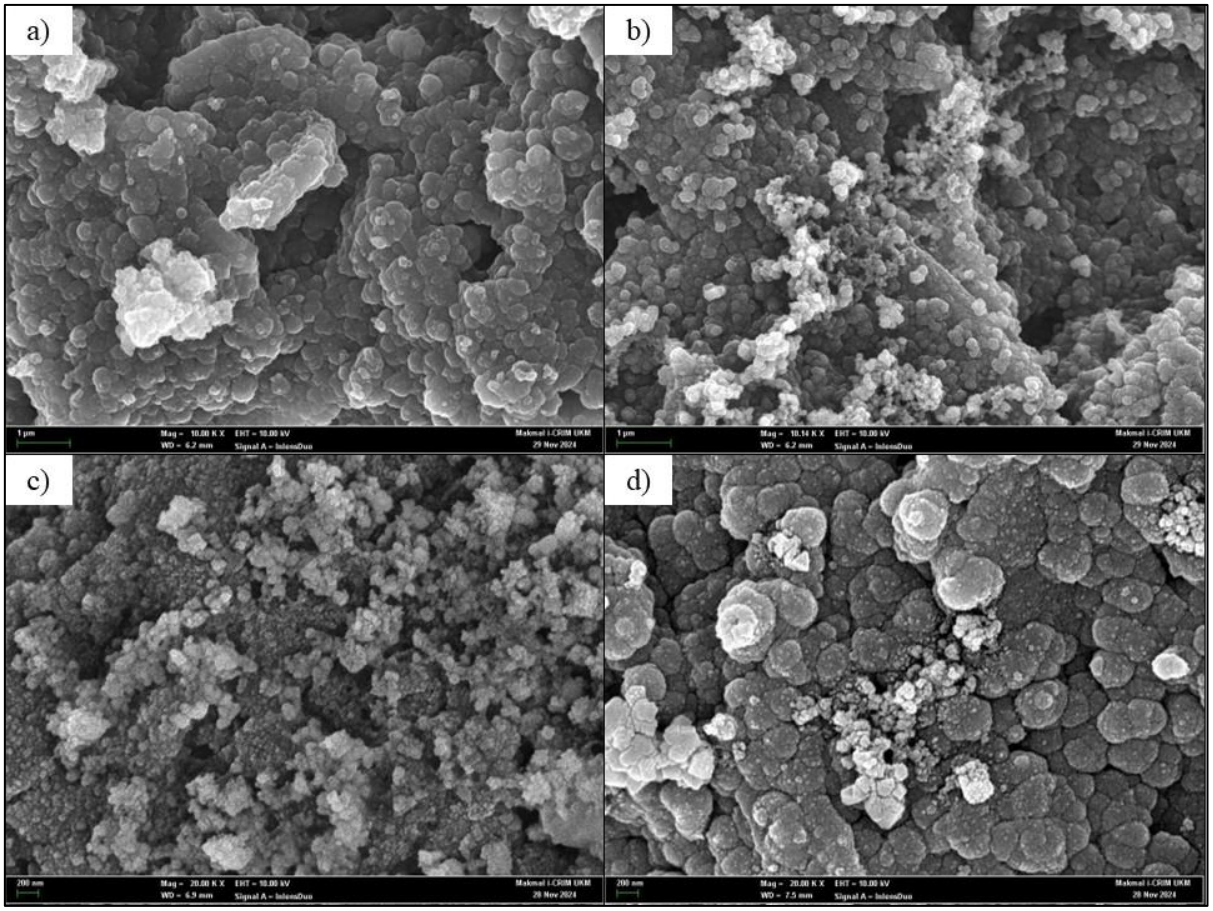

Figure 4. SEM morphology of a) leached e-NIP, b) incubated e-NIP, c) leached e-MIP and d) incubated e-MIP.

Following target rebinding, the incubated e-MIP (Figure 4d) exhibited visibly occupied and partially occluded pores compared to its finely structured leached counterpart, forming denser agglomerates. This morphological shift provides direct visual evidence that the oxybenzone molecules successfully re-entered and saturated the specific cavities within the polypyrrole matrix. Ultimately, these distinct morphological differences vividly illustrate the imprinting effect and strongly support the superior electrochemical selectivity and signal enhancement observed for the e-MIP sensor.

Optimization of Experimental Conditions

To ensure maximum sensitivity and analytical performance of the fabricated e-MIP sensor, critical operational parameters, specifically the target incubation time and supporting electrolyte pH, were systematically optimized.

The binding kinetics between the target analyte and the e-MIP cavities were evaluated by tracking the electrochemical response across incubation periods ranging from 5 to 25 minutes. As illustrated in Figure 5, the anodic peak current increased steadily over the first 10 minutes, reflecting the progressive diffusion and specific adsorption of oxybenzone into the complementary recognition sites at the electrode interface. The maximum signal was recorded at exactly 10 minutes, indicating that thermodynamic equilibrium for the analyte-receptor complex had been successfully established.

Prolonging the incubation time beyond this optimal window led to a gradual decrease in the current response. This reduction is likely caused by the complete saturation of the specific binding cavities, which may subsequently trigger competitive non-specific surface adsorption or steric hindrance effects that ultimately occlude the electroactive surface and restrict further electron transfer [36]. Consequently, to ensure rapid and highly sensitive detection, 10 minutes was selected as the optimal incubation time for all subsequent analytical measurements.

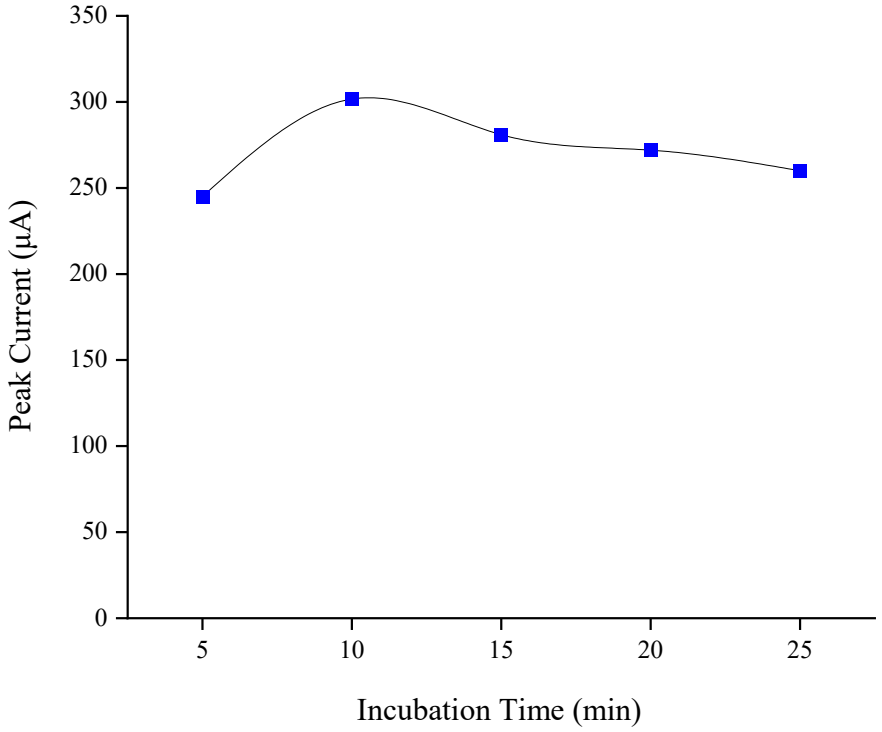

Figure 5. Effect of analyte incubation time on the electrochemical binding response of the e-MIP sensor toward oxybenzone.

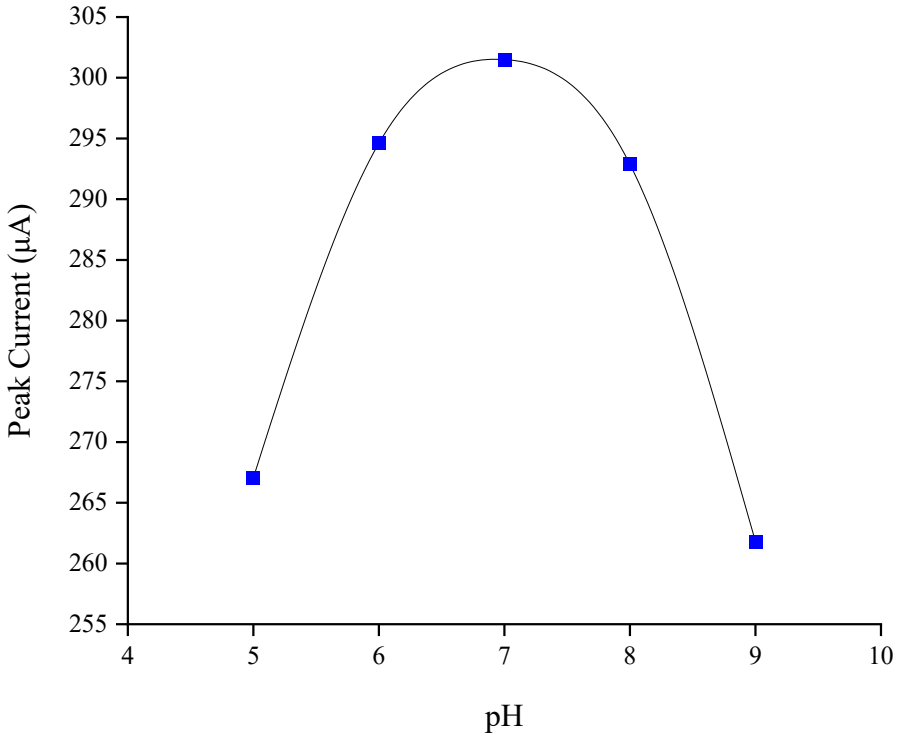

Figure 6. Influence of the supporting electrolyte pH on the oxidation peak current of the e-MIP sensor.

The pH of the supporting electrolyte fundamentally influences the sensor's performance by altering both the charge state of the target analyte and the structural conformation of the polypyrrole matrix. As illustrated in Figure 6, the oxidation peak current exhibited a distinct bell-shaped profile, achieving its maximum analytical response at a neutral pH of 7. Deviations from this optimal neutral environment resulted in a significant decrease in the current response. Under acidic conditions (pH < 7), extensive protonation occurs on the functional groups of both the oxybenzone molecules and the polymer matrix. This protonation disrupts the critical hydrogen bonding networks essential for specific target recognition, thereby diminishing the overall binding efficiency [36]. Conversely, the sharp decline in the analytical signal in basic environments (pH > 7) is directly correlated to the acid dissociation constant (pKa) of oxybenzone, which is 7.1 [37]. In regimes exceeding this pKa, oxybenzone undergoes deprotonation, shifting from a neutral molecule to an anionic form. This induced negative charge generates strong electrostatic repulsions between the analyte and the similarly charged polymer surface, rendering the molecule electronically incompatible with the imprinted cavities and severely impairing binding efficiency. Furthermore, prolonged exposure to extreme acidic or alkaline levels can severely compromise the intrinsic stability of conducting polymers like polypyrrole, leading to structural distortion, cavity collapse, and a subsequent irreversible loss of electrochemical activity [8]. This vulnerability underscores the necessity of operating within the optimized, neutral parameters established in this study.

Analytical Performance of the e-MIP Sensor

To evaluate the quantitative analytical performance of the fabricated e-MIP sensor, electrochemical measurements were recorded across varying concentrations of the oxybenzone target. Following the optimized 10-minute incubation period, the sensor exhibited a proportional increase in the faradaic oxidation peak current as the analyte concentration increased. This positive correlation corroborates the direct detection mechanism established earlier; higher target concentrations lead to increased occupancy of the imprinted cavities, resulting in enhanced localized accumulation and subsequent direct oxidation of oxybenzone at the electrode interface.

As depicted in the calibration plot (Figure 7), the sensor demonstrated a linear response range from 5 mM to 25 mM. The linear regression equation was established as $I\ (\mu A) = 12.018\ C_{oxybenzone} + 25.47$, with a highly satisfactory correlation coefficient (R^2) of 0.9864. Based on the standard deviation of the blank response (S/N = 3), the LOD was calculated to be 4.80 mM, while the LOQ was determined to be 14.5 mM.

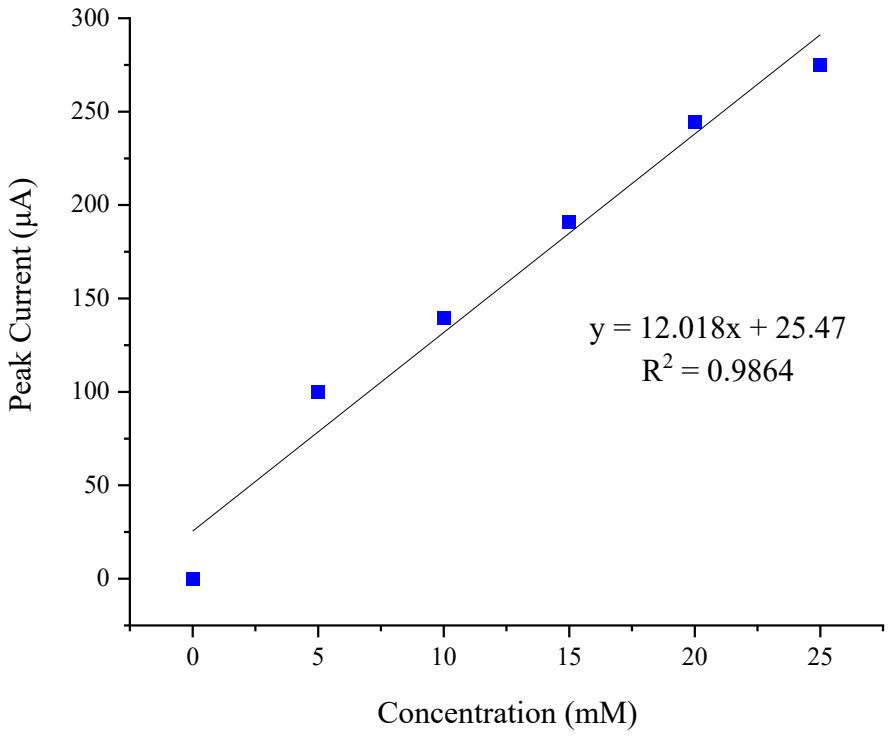

Figure 7. Calibration curve demonstrating the linear relationship between the faradaic peak current and oxybenzone concentration (5.0 to 25.0 mM) under optimized operational conditions.

Table 1. Comparison of the analytical performance of the proposed e-MIP sensor with previously reported electrochemical sensors.

Electrode Modification	Target Analyte	Linear Range	Limit of Detection (LOD)	Reference
MIP / EIS	Oxybenzone	0.043 – 4.38 µM	0.17 µM	[32]
FeCu-MOF/RGO/PDA@MXene	Ribavirin	0.41 – 40.9 µM	0.065 µM	[15]
eMIP@PPy/SPGE	Oxybenzone	0.01 – 10 µM	13.2 µM	[19]
e-MIP/SPCE	Oxybenzone	5 – 25 mM	4.80 mM	This work

To contextualize the efficacy of the proposed e-MIP sensor, its analytical metrics were compared against previously reported electrochemical platforms (Table 1). Recent advancements in oxybenzone detection have achieved trace-level sensitivity. For instance, an impedance-based MIP sensor reported an LOD of 0.17 µM [39], while an imprinted screen-printed gold electrode (eMIP@PPy/SPGE) reached 13.2 µM [19]. Similarly, advanced modifications for related endocrine-disrupting compounds, such as complex nanocomposite functionalization (e.g., FeCu-MOF/RGO/PDA@ MXene), exhibit ultra-low detection limits but frequently require resource-intensive and highly expensive fabrication processes [40].

However, the proposed e-MIP platform deliberately trades trace-level sensitivity for a much simpler and more cost-effective carbon substrate. By leveraging a straightforward "green" electropolymerization methodology [25], this sensor offers a highly practical, scalable alternative [41]. Although the current LOD is suited for environments with elevated contamination levels, such as direct industrial effluents or cosmetic manufacturing runoff, rather than trace environmental monitoring, the inherent portability and low cost of SPCEs establish this platform as a valuable proof-of-concept for routine, on-site industrial screening.

Repeatability and Imprinting Factor

The practical reliability and robustness of the fabricated e-MIP sensor were evaluated through repeatability studies under optimized conditions. Four successive measurements of the target analyte yielded a highly consistent electrochemical response, generating an average faradaic peak current of 295.95 µA with a standard deviation of 8.09 µA and a relative standard deviation (RSD) of 3.0 %. An RSD below 5 % is widely recognized as the benchmark for acceptable precision in electrochemical sensing [42, 43]. This low value demonstrates the excellent structural stability of the electropolymerized film and confirms that the sensor provides highly reproducible analytical outputs suitable for routine monitoring.

To quantitatively assess the specific recognition capabilities generated by the imprinting process, the imprinting factor (IF) was evaluated. The IF is defined as the ratio of the peak current response of the imprinted polymer to that of the non-imprinted control ($IF = I_{MIP}/ I_{NIP}$) [43]. As summarized in Table 2, the e-MIP exhibited a strong peak current of 310.00 µA toward oxybenzone, whereas the e-NIP recorded a significantly lower response of 190.00 µA. This yielded an IF of 1.63, confirming that the tailored recognition cavities within the e-MIP matrix successfully enhanced the sensor's affinity and binding capacity for the target analyte, surpassing the non-specific surface adsorption observed on the e-NIP control.

Table 2. Selectivity profile and imprinting factor of the e-MIP and e-NIP modified electrodes.

Sensor Type	Peak Current (µA)	Imprinting Factor (IF)
e-NIP	190.00	-
e-MIP	310.00	1.63

CONCLUSION

A selective electrochemical sensor for the direct detection of oxybenzone was successfully developed using an electropolymerized molecularly imprinted polymer (e-MIP) on a SPCE. The facile, one-step electropolymerization of pyrrole, followed by template leaching, effectively generated tailored recognition cavities specific to oxybenzone, as corroborated by FTIR, SEM, and electrochemical characterizations. Systematic optimization of the operational parameters, specifically incubation time and pH, maximized the sensor's analytical capabilities. The optimized e-MIP sensor demonstrated a reliable linear relationship for oxybenzone concentrations ranging from 5.0 to 25.0 mM, achieving a practical LOD of 4.80 mM. Additionally, the sensor exhibited excellent repeatability and a strong imprinting factor (IF = 1.63), confirming its superior specificity and targeted binding capacity compared to the non-imprinted control.

By leveraging the inherent advantages of SPCEs, this study presents a practical, cost-effective, and portable platform that holds significant promise for the routine, on-site screening of oxybenzone at elevated contamination levels. While the current detection range is calibrated for highly concentrated industrial effluents or stock formulations, future sensor iterations will focus on signal amplification to monitor trace-level environmental concentrations or the efficiency of emerging wastewater remediation technologies. Bridging this sensitivity gap through nanomaterial integration or multi-template imprinting strategies could enable the simultaneous trace-level detection of oxybenzone alongside other co-occurring UV filters, providing a comprehensive and scalable tool for the analysis of complex environmental matrices.

ACKNOWLEDGEMENTS

The authors gratefully acknowledge the financial support provided by the Talent and Publication Enhancement Research Grant (UMT/TAPE-RG/2025/55629). Sincere appreciation is also extended to Universiti Malaysia Terengganu for providing the essential laboratory facilities, instruments, and technical support required to successfully conduct this research.

REFERENCES

1. Wang, H., Hu, L., Liu, X., Yin, S., Lu, R., Zhang, S., Zhou, W. and Gao, H. (2017) Deep eutectic solvent-based ultrasound-assisted dispersive liquid-liquid microextraction coupled with high-performance liquid chromatography for the determination of ultraviolet filters in water samples. *Journal of Chromatography A*, **1516**, 1–8.

2. Celeiro, M., Acerbi, R., Kabir, A., Furton, K.G. and Llompart, M. (2020) Development of an analytical methodology based on fabric phase sorptive extraction followed by gas chromatography-tandem mass spectrometry to determine UV filters in environmental and recreational waters. *Analytica Chimica Acta: X*, **4**, 100038.

3. Magrin, C.P., Cardoso, C. dos S., Pereira-Coelho, M., Vitali, L., Maranhão, T. de A. and Micke, G.A. (2025) Development of a dispersive pipette extraction method for the determination of eleven sunscreen molecules in seawater samples. *Microchemical Journal*, **209**, 112817.

4. Ren, S., Dong, F., Liu, J., Bekele, T.G., Wang, Y., Zhao, H., Chen, J., Tan, F. and Wang, X. (2022) Development of diffusive gradients in thin film technique for seasonal monitoring of benzophenone-type UV filters in coastal waters. *Water Research*, **222**, 118944.

5. Loos, R., Tavazzi, S., Paracchini, B., Canuti, E. and Weissteiner, C. (2013) Analysis of polar organic contaminants in surface water of the northern Adriatic Sea by solid-phase extraction followed by ultrahigh-pressure liquid chromatography-QTRAP® MS using a hybrid triple-quadrupole linear ion trap instrument. *Analytical and Bioanalytical Chemistry*, **405**, 5875–5885.

6. Abaroa-Pérez, B., Sánchez-Almeida, G., Hernández-Brito, J.J. and Vega-Moreno, D. (2018) In Situ Miniaturised Solid Phase Extraction (m-SPE) for Organic Pollutants in Seawater Samples. *Journal of Analytical Methods in Chemistry*, **2018**, 7437031.

7. Li, M. and Guo, L.H. (2023) Chemo/biosensors towards effect-directed analysis: An overview of current status and future development. *TrAC - Trends in Analytical Chemistry*, **158**, 116824.

8. Sawant, S.S., Bharti, V.S., Shukla, S.P., Verma, A.K., Yadav, V.K. and Shinde, S. (2025) Integrated biochar and Lemna minor system for sustainable remediation of Benzophenone-3 from wastewater. *Scientific Reports*, **15**, 40329.

9. Bou-Maroun, E. (2023) Carbon Electrode Modified with Molecularly Imprinted Polymers for the Development of Electrochemical Sensor: Application to Pharmacy, Food Safety, Environmental Monitoring, and Biomedical Analysis. *Chemosensors*, **11**, 548.

10. Mayes, A.G. and Whitcombe, M.J. (2005) Synthetic strategies for the generation of molecularly imprinted organic polymers.

Advanced Drug Delivery Reviews, **57**, 1742–1778.

11. Erdem, A., Senturk, H. and Karakus, M. (2025) Molecularly imprinted polymer-based sensors: Design and advances in the analysis of DNA and protein. *Talanta Open*, **12**, 100507.

12. Han, Y., Tao, J., Ali, N., Khan, A., Malik, S., Khan, H., Yu, C., Yang, Y., Bilal, M. and Mohamed, A.A. (2022) Molecularly imprinted polymers as the epitome of excellence in multiple fields. *European Polymer Journal*, **179**, 111582.

13. Chen, M., Li, H., Xue, X., Tan, F. and Ye, L. (2024) Signal amplification in molecular sensing by imprinted polymers. *Microchimica Acta*, **191**, 574.

14. Díaz-Álvarez, M., Turiel, E. and Martín-Esteban, A. (2023) Recent advances and future trends in molecularly imprinted polymers-based sample preparation. *Journal of Separation Science*, **46**, 2300157.

15. Bravo-Yagüe, J.C., Paniagua-González, G., Garcinuño, R.M., García-Mayor, A. and Fernández-Hernando, P. (2025) Colorimetric Molecularly Imprinted Polymer-Based Sensors for Rapid Detection of Organic Compounds: A Review. *Chemosensors*, **13**, 163.

16. Blel, A., Karrat, A., Mrabet, W., Amine, A. and Dridi, C. (2025) Improving MIP-based electrochemical sensors by minimizing non-specific adsorption. *Microchemical Journal*, **218**, 115115.

17. Oliveira, S.M., Luzardo, J.M., Silva, L.A., Aguiar, D.C., Senna, C.A., Verdan, R., Kuznetsov, A., Vasconcelos, T.L., Archanjo, B.S., Achete, C.A., D'Elia, E. and Araujo, J.R. (2020) High-performance electrochemical sensor based on molecularly imprinted polypyrrole-graphene modified glassy carbon electrode. *Thin Solid Films*, **699**, 137875.

18. Hasanova, S., Ait Lahcen, A. and Zor, E. (2024) Recent advances in molecular imprinting techniques for the electrochemical analysis of chiral compounds. *Journal of Pharmaceutical and Biomedical Analysis Open*, **4**, 100046.

19. Jamilan, M.A., Kanthymathynathan, V., Mehamod, F.S. and Md Noh, M.F. (2026) Electrochemical sensor detection of oxybenzone using an in situ molecularly-imprinted polypyrrole modified screen printed gold electrode. *Pure and Applied Chemistry*, **0**.

20. Ben Moussa, F., Beduk, T., Sena-Torralba, A., Beduk, D., Ait Lahcen, A., Kutner, W. and Kaushik, A. (2025) Beyond single-analyte detection: Advancing molecularly imprinted polymers for simultaneous multi-target sensing. *TrAC - Trends in Analytical Chemistry*, **185**, 118177.

21. Poza-Nogueiras, V., Puga, A., Pacheco, J.G. and Delerue-Matos, C. (2026) Rapid carbamazepine detection by means of a disposable electrochemical sensor based on a molecularly imprinted polymer. *Talanta*, **299**, 129128.

22. Andrieux, C.P., Audebert, P., Hapiot, P. and Savéant, J.-M. (1991) Identification of the First Steps of the Electrochemical Polymerization of Pyrroles by Means of Fast Potential Step Techniques. *The Journal of Physical Chemistry*, **95**, 10158–10164.

23. Sharma, P.S., Pietrzyk-Le, A., D'Souza, F. and Kutner, W. (2012) Electrochemically synthesized polymers in molecular imprinting for chemical sensing. *Analytical and Bioanalytical Chemistry*, **402**, 3177–3204.

24. Dhaffouli, A. (2026) Next-generation antifouling electrochemical sensors: From surface design to practical applications. *Microchemical Journal*, **220**, 116637.

25. Aoulad El Hadj Ali, Y., Hejji, L., Ait Lahcen, A., Pérez-Villarejo, L., Azzouz, A. and Kim, K.H. (2024) Progress and prospects in the green synthesis of molecularly imprinted polymers for sorptive extraction and sensing applications toward emerging contaminants in various sample matrices. *Trends in Analytical Chemistry*, **170**, 117466.

26. Kassar, M., Singh, I., Bauer, M., Ballweg, T., Thelen, R., Franzreb, M. and Kabay, G. (2025) Polybithiophene-Based Molecularly Imprinted Polymers: A Comparative Mechanistic Study on Electrochemical Signal Transduction Approaches for Protein Detection. *Advanced Sensor Research*, **4**, e00104.

27. Pereira, A.C., Braga, G.B., Oliveira, A.E.F., Silva, R.C. and Borges, K.B. (2019) Synthesis and characterization of molecularly imprinted polymer for ethinylestradiol. *Chemical Papers*, **73**, 141–149.

28. Hanun, J.N., Hassan, F., Theresia, L., Chao, H.R., Bu, H.M., Rajendran, S., Kataria, N., Yeh, C.F., Show, P.L., Khoo, K.S. and Jiang, J.J. (2023) Weathering effect triggers the sorption enhancement of microplastics against oxybenzone. *Environmental Technology and Innovation*, **30**, 103112.

29. Zhang, M., Yang, Y., Wang, Y., Zhang, B., Wang, H., Fang, G. and Wang, S. (2022) A molecularly imprinted electrochemical sensor based on cationic intercalated two-dimensional titanium carbide nanosheets for sensitive and selective detection of triclosan in food samples. *Food Control*, **132**, 108532.

30. Kalogiouri, N.P., Kabir, A., Furton, K.G. and Samanidou, V.F. (2025) A tutorial on the synthesis and applications of molecularly imprinted polymers in analytical chemistry. *Journal of Chromatography Open*, **8**, 100244.

31. Al-Saeedi, F.M.A.A. and Dahmash, E.Z. (2022) In Vitro Assessment of Sunscreen Efficacy Using Fourier Transform Infrared (FTIR) Spectroscopy on Synthetic Skin. *AAPS PharmSciTech*, **23**, 73.

32. Essousi, H., Wannassi, J., Elloumi, A., Ali, E. and Barhoumi, H. (2025) Electrochemical sensor of oxytetracycline based on molecularly imprinted poly(3,4-ethylenedioxythiophene)/MXene on graphene screen printed electrode. *Microchemical Journal*, **215**, 114425.

33. El Jaouhari, A., Yan, L., Zhu, J., Zhao, D., Hossain Khan, M.Z. and Liu, X. (2020) Enhanced molecular imprinted electrochemical sensor based on zeolitic imidazolate framework/reduced graphene oxide for highly recognition of rutin. *Analytica Chimica Acta*, **1106**, 103–114.

34. Wang, H., He, Y., Wang, R., Lu, M., Luo, Y., Sun, Y. and Xu, D. (2025) An electrochemical sensor of PBA-grafted Zn-MOF/MIP for sensitive rutin detection. *Microchemical Journal*, **215**, 114145.

35. Zhou, Y., Abdurexit, A., Jamal, R., Abdiryim, T., Liu, X., Liu, F., Xu, F., Zhang, Y. and Wang, Z. (2024) Highly sensitive electrochemical sensing of norfloxacin by molecularly imprinted composite hollow spheres. *Biosensors and Bioelectronics*, **251**, 116119.

36. Sharma, P.S., Dabrowski, M., D'Souza, F. and Kutner, W. (2013) Surface development of molecularly imprinted polymer films to enhance sensing signals. *TrAC - Trends in Analytical Chemistry*, **51**, 146–157.

37. Susanti, I. and Hasanah, A.N. (2021) How to develop molecularly imprinted mesoporous silica for selective recognition of analytes in pharmaceutical, environmental, and food samples. *Polymers for Advanced Technologies*, **32**, 1965–1980.

38. Brazys, E., Ratautaite, V., Mohsenzadeh, E., Boguzaite, R., Ramanaviciute, A. and Ramanavicius, A. (2025) Formation of molecularly imprinted polymers: Strategies applied for the removal of protein template (review). *Advances in Colloid and Interface Science*, **337**, 103386.

39. Sarti, C., Falcon, L., Cincinelli, A., Martellini, T. and Chianella, I. (2025) Development of molecularly imprinted polymer-based electrochemical sensors for the detection of UV filters in aquatic ecosystems. *Talanta*, **285**, 127375.

40. Gao, H., You, J., Wu, H. and Tian, M. (2025) A dual action electrochemical molecular imprinting sensor based on FeCu-MOF and RGO/PDA@MXene hybrid synergies for trace detection of ribavirin. *Food Chemistry*, **473**, 143092.

41. Zhang, W., Liu, C., Han, K., Wei, X., Xu, Y., Zou, X., Zhang, H. and Chen, Z. (2020) A signal on-off ratiometric electrochemical sensor coupled with a molecular imprinted polymer for selective and stable determination of imidacloprid. *Biosensors and Bioelectronics*, **154**, 112091.

42. Zeng, D., Zhong, B., Zhou, T., Yu, C., Jiang, S., Chen, J. and Song, Y. (2024) A development of sensor based on ZnO@ZIF-8 for detection of 5-Fluorouracil as a liver cancer medicine in serum samples. *Inorganic Chemistry Communications*, **170**, 113179.

43. Wang, Y., Yao, L., Liu, X., Cheng, J., Liu, W., Liu, T., Sun, M., Zhao, L., Ding, F., Lu, Z., Zou, P., Wang, X., Zhao, Q. and Rao, H. (2019) CuCo2O4/N-Doped CNTs loaded with molecularly imprinted polymer for electrochemical sensor: Preparation, characterization and detection of metronidazole. *Biosensors and Bioelectronics*, **142**, 111483.